*Wind and Structures, Vol. 7, No. 2 (2004) 107-130*
DOI: http://dx.doi.org/10.12989/was.2004.7.2.107


# Monte Carlo simulation for the response analysis of long-span suspended cables under wind loads

M. Di Paola†

*Dipartimento di Ingegneria Strutturale e Geotecnica, Università di Palermo, Viale delle Scienze, 90128, Palermo, Italy*

G. Muscolino† and A. Sofi‡

*Dipartimento di Costruzioni e Tecnologie Avanzate, Università di Messina, Salita Sperone 31, 98166, S.Agata-Messina, Italy*

*(Received March 1, 2003, Accepted December 10, 2003)*

**Abstract.** This paper presents a time-domain approach for analyzing nonlinear random vibrations of long-span suspended cables under transversal wind. A consistent continuous model of the cable, fully accounting for geometrical nonlinearities inherent in cable behavior, is adopted. The effects of spatial correlation are properly included by modeling wind velocity fluctuation as a random function of time and of a single spatial variable ranging over cable span, namely as a one-variate bi-dimensional (1V-2D) random field. Within the context of a Galerkin's discretization of the equations governing cable motion, a very efficient Monte Carlo-based technique for second-order analysis of the response is proposed. This procedure starts by generating sample functions of the generalized aerodynamic loads by using the spectral decomposition of the cross-power spectral density function of wind turbulence field. Relying on the physical meaning of both the spectral properties of wind velocity fluctuation and the mode shapes of the vibrating cable, the computational efficiency is greatly enhanced by applying a truncation procedure according to which just the first few significant loading and structural modal contributions are retained.

**Keywords:** suspended cable; wind velocity; random field; digital simulation; Proper Orthogonal Decomposition; nonlinear vibrations.

## 1. Introduction

Due to their light weight associated with great flexibility and low structural damping, suspended cables are prone to large amplitude vibrations under external and parametric excitations. Theoretical and experimental investigations have shown that the issues related to wind-induced oscillations of cables are of great concern at the design stage, in order to prevent damage and fatigue problems of cable structures and overhead transmission lines. Such problems are mainly caused by typical instability phenomena like rain-wind induced vibrations, vortex-shedding, galloping, etc.

In some recent works, dealing with cable oscillations under wind loading, consistent mechanical

† Professor
‡ Research Fellow

models of the cable able to include both geometrical and aerodynamic nonlinearities, have been adopted (Desai, *et al*. 1995, Luongo, *et al*. 1998, Pasca, *et al.* 1998, Gattulli, *et al*. 2001, Martinelli, *et al.* 2002, Carassale and Piccardo 2003).

In view of the inherent nonlinearities, Monte Carlo simulation (MCS) technique may be regarded as the only accurate and versatile tool so far available for analyzing random vibrations of wind-excited cables. A key step of any Monte Carlo-based procedure is the numerical simulation of time-histories of input processes with given spectral density distribution. The cross-correlation between wind velocity fluctuations at different point locations of extended wind-exposed structures requires the use of appropriate tools for digital simulation of the ensuing aerodynamic forces. Many authors tackled the problem assuming the loads concentrated at scattered points of the structure. This is achieved by discretizing the stationary Gaussian random field modeling wind turbulence into an *n*V-1D stochastic process, i.e., an *n*-vector collecting 1V-1D processes (depending only on time), which represent the realizations of wind velocity fluctuation at *n* selected points of the structure. In the same way, the Cross-Power Spectral Density (CPSD) function of the turbulence field is discretized into a matrix of order *n*, providing the complete probabilistic characterization of the normal *n*V-1D stochastic process.

Basically, two classes of techniques are commonly used for digital simulation of stationary Gaussian *n*V-1D random processes: the wave-superposition-based methods (see e.g., Shinozuka 1971, Shinozuka and Jan 1972, Grigoriu 1993, Deodatis 1996, Shinozuka and Deodatis 1996) and the time series approaches, which include the auto-regressive (AR) and auto-regressive moving average (ARMA) algorithms (see e.g., Spanos and Mignolet 1986, Naganuma, *et al.* 1987, Deodatis and Shinozuka 1988, Li and Kareem 1990). The first methods require the repetitive factorization of the CPSD matrix at each frequency step, which is usually performed by means of Cholesky decomposition. The most important issue in practical applications of spectral methods concerns the computation speed and the storage requirements as the number of simulation points increases. On the other hand, the main drawback of time series approaches is the difficulty in choosing a suitable model order to obtain good match with the target flow properties. Several improved algorithms have been proposed to enhance the computational efficiency of both spectral approaches and ARMA-based techniques. In this regard, it has to be mentioned that the Proper Orthogonal Decomposition (POD) (Loeve 1955, Papoulis 1965) represents an effective tool to overcome the severe limitations imposed on the number of simulation points. The POD expresses a multi-dimensional/variate random process as summation of fully coherent component processes uncorrelated in some statistical sense, which are referred to as modes of the process. Li and Kareem (1993, 1995) proposed an approach based on stochastic decomposition, which transforms the original space to one in which the component processes are either fully coherent or non-coherent. Furthermore, through the joint application of the POD and classical modal analysis, a technique called Double Modal Transformation (DMT) has been set up to evaluate the dynamic response of linear structures subjected to random loads (Carassale, *et al.* 2001). Recently, the POD has been successfully applied to develop a very efficient wave-superposition-based technique for digital simulation of multivariate wind velocity processes (Di Paola 1998, Di Paola and Gullo 2001). This procedure expresses the target process as a summation of fully coherent independent stochastic processes, taking full advantage of the decomposition of the CPSD matrix into the frequency-dependent basis of its eigenvectors. The attractiveness of this particular choice lies in the meaningful physical interpretation of the eigenproperties of the CPSD matrix. Within a continuous formulation, the POD of a bi-dimensional non-homogeneous process has also been employed in a recent work (Carassale and Solari 2002) for the evaluation of the dynamic response of wind-excited mono-dimensional linear structures.

In the present work, second-order analysis of nonlinear in-plane and out-of-plane random vibrations of long-span suspended cables under transversal wind is carried out by extending a simulation technique recently proposed by the authors (Di Paola, *et al.* 2002) for shallow cables on the left of the first crossover point (Irvine 1981). This procedure stems from the application of DMT concept within a nonlinear setting. Since to the authors' knowledge, DMT method has been so far applied to linear problems only, one of the main purposes of the paper is to investigate the performances of such approach in the dynamic analysis of nonlinear structures under stochastic excitation. The cable is modeled as a mono-dimensional elastic continuum, fully accounting for geometrical nonlinearities (Luongo, *et al.* 1984). By referring the analysis to flat-sag cables, which may be reasonably regarded as horizontal string-like exposed structures, wind velocity fluctuation is treated as a one-variate bi-dimensional (1V-2D) zero-mean Gaussian random field (depending on time and a single spatial variable ranging over the span), stationary in time and isotropic in space. The aerodynamic forces are defined referring to a spring-mounted damped rigid cylinder of indefinite length in the quasi-static regime (i.e., at much lower oscillation frequencies than the vortex-shedding frequency (Simiu and Scanlan 1996)), under the assumption of small turbulence with respect to the mean wind component (Piccardo 1993). Numerical investigations have demonstrated that the influence of nonlinear aerodynamic terms on first and second-order statistical moments of cable response is negligible. Since the proposed approach is aimed at second-order analysis of wind-induced cable vibrations, linearized expressions of the aerodynamic forces (Pasca, *et al.* 1998) are here assumed in order to simplify the theoretical formulation and reduce the computational effort. The time-domain analysis of cable response is carried out by Galerkin's method, expressing the displacement components in terms of eigenfunctions of the associated linear problem and generalized coordinates. Following closely the wave-superposition-based approach proposed in Refs. (Di Paola 1998, Di Paola and Gullo 2001) for multivariate 1D processes, a very efficient technique for digital simulation of the generalized aerodynamic loads is developed starting from the POD of wind turbulence field into the basis of the frequency-dependent eigenfunctions of the CPSD function. The joint application of the POD of wind velocity fluctuation and Galerkin's method provides considerable computational savings in buffeting response analysis of long-span suspended cables. In particular, the physical meaning of both the eigenproperties of the CPSD function and the mode shapes of the vibrating cable suggests a natural truncation procedure according to which just the first few significant loading and structural modal contributions are retained.

Some numerical results concerning two cables with different geometrical and mechanical properties are presented. Beside the accuracy and efficiency of the simulation technique developed in the paper, the appropriate selection of the order of the discretized model and the effect of spatial correlation of wind turbulence on cable vibrations are also examined.

## 2. Suspended cable under turbulent wind: continuous formulation

### 2.1. Cable model

Consider a uniform elastic cable hanging under its own weight between two fixed level supports subjected to turbulent transversal wind (Fig. 1). Let $Oxyz$ be a Cartesian coordinate system with origin $O$ at the left-hand support of the cable ($O \equiv A$) and the $z$ axis aligned with the mean wind direction. Following the Lagrangean approach, cable motion is referred to the initial static

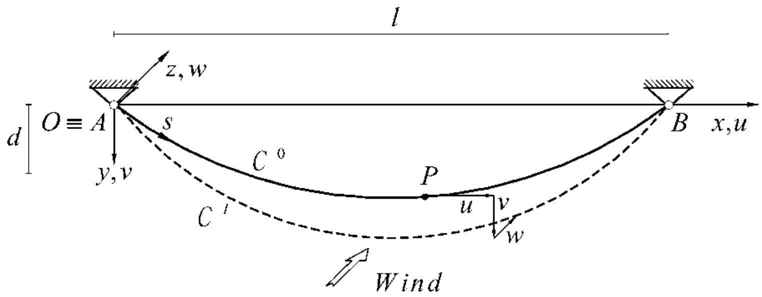


Fig. 1 Suspended cable under transversal wind

equilibrium configuration $\mathcal{C}^0$, which lies in the vertical plane ($Oxy$) and is represented by the function $y(s)$, $s \in [0, l_c]$ being a curvilinear abscissa and $l_c$ the unstretched cable length. The varied configuration $\mathcal{C}^I$ under external excitation is described by the dynamic displacement components $u(s,t)$, $v(s,t)$ and $w(s,t)$ of a given point $P(s)$, measured from the initial undisturbed configuration $\mathcal{C}^0$ along the coordinate axes $x$, $y$ and $z$, respectively.

By referring the analysis to shallow cables, namely those with small sag-to-span ratio, $d/l$, (i.e., $d/l \leq 1/8$ (Irvine 1981)), a curvilinear element d$s$ can be approximated with d$x$. Consequently, the static equilibrium configuration $\mathcal{C}^0$ can be adequately described through the parabolic profile $y(x)=4d[x/l-(x/l)^2]$, which in turn implies a constant static tension equal to its horizontal component $N_0(s) \cong H$. Furthermore, the following assumptions are introduced (Luongo, *et al.* 1984): i) the gradient of the horizontal component of the dynamic displacement is negligible with respect to unity, i.e., moderately large rotations occur in the motion; ii) the initial strain is negligible with respect to unity, which entails $H/EA \ll 1$, where $E$ and $A$ denote the modulus of elasticity and the cross-sectional area of the cable, respectively.

Under the previous assumptions, the extended Hamilton's principle yields the following set of nonlinear coupled partial differential equations, governing wind-induced cable vibrations referenced to the configuration $\mathcal{C}^0$ (Pasca, *et al.* 1998):

$$m\ddot{u}(x, t) + \mu_u \dot{u}(x, t) - [EA\varepsilon(x, t)]' = 0 \tag{1}$$

$$m\ddot{v}(x, t) + \mu_v \dot{v}(x, t) - \{Hv'(x, t) + EA[y'(x) + v'(x, t)]\varepsilon(x, t)\}' = f_y(x, t) \tag{2}$$

$$m\ddot{w}(x, t) + \mu_w \dot{w}(x, t) - \{w'(x, t)[H + EA\varepsilon(x, t)]\}' = f_z(x, t) \tag{3}$$

where a dot and a prime indicate derivative with respect to time $t$ and abscissa $x$, respectively; $m$ is the cable mass per unit length; $\mu_u$, $\mu_v$ and $\mu_w$ are the damping coefficients of the cable; $f_y(x,t)$ and $f_z(x,t)$ denote the aerodynamic loads along the $y$ and $z$ directions, whose explicit expressions will be given in the next section; at last, $\varepsilon(x,t)$ is the Lagrangean strain, defined as follows:

$$\varepsilon(x, t) = u'(x, t) + y'(x)v'(x, t) + \frac{1}{2}[v'^2(x, t) + w'^2(x, t)] \tag{4}$$

Eqs. (1)-(3) are supplemented by homogeneous boundary conditions in [0, $l$].

In view of the assumptions on cable geometry previously introduced, the inertial term $m\ddot{u}(x,t)$ in Eq. (1) can be neglected and the horizontal displacement component $u(x,t)$ can be eliminated by a standard condensation procedure. So operating, the elongation turns out to be a function of time alone, given by:

$$\varepsilon^{(c)}(t) = \frac{1}{l}\int_0^l \left\{ y'(x)v'(x,t) + \frac{1}{2}[v'^2(x,t) + w'^2(x,t)] \right\} \mathrm{d}x \tag{5}$$

where the superscript in parentheses stands for "condensed".

Substituting the previous relation into Eqs. (2) and (3), the following two reduced partial integro-differential equations in the transversal displacement components $v(x,t)$ and $w(x,t)$ are recovered:

$$m\ddot{v}(x,t) + \mu_v \dot{v}(x,t) - \{Hv'(x,t) + EA[y'(x) + v'(x,t)]\varepsilon^{(c)}(t)\}' = f_y(x,t) \tag{6}$$

$$m\ddot{w}(x,t) + \mu_w \dot{w}(x,t) - \{w'(x,t)[H + EA\varepsilon^{(c)}(t)]\}' = f_z(x,t) \tag{7}$$

Eqs. (6) and (7) contain both quadratic and cubic nonlinearities, which are due to initial curvature and cable stretching, respectively. The aforementioned equations are accurate for studying suspended cables used in overhead transmission lines.

### *2.2. Stochastic modeling of wind loads*

Once a consistent continuous model of the suspended cable, fully accounting for geometrical nonlinearities, has been defined, the aerodynamic loads, $f_y(x,t)$ and $f_z(x,t)$ (see Eqs. (6) and (7)), need to be properly characterized on the basis of a realistic model of natural wind.

Neglecting the contribution of the horizontal and vertical turbulence fluctuations, the instantaneous wind velocity is defined just by its component in the along-wind direction ($z$ axis), i.e.:

$$W(x,t) = \overline{W}(h) + \tilde{W}(x,t) \tag{8}$$

where the first and second term on the right-hand side represent the mean and fluctuation, respectively. The mean wind velocity $\overline{W}(h)$ is modeled as a deterministic function of the height $h$ above ground, measured at the level supports ($A$ and $B$). The fluctuating component $\tilde{W}(x,t)$ is treated as a random function of time $t$ and the spatial variable $x \in [0,l]$, namely as a one-variate bi-dimensional (1V-2D) stationary zero-mean Gaussian random field, whose complete probabilistic characterization is ensured by the knowledge of the Cross-Power Spectral Density (CPSD) function. If $x_j$ and $x_k$ are the abscissas of two different point locations $P_j$ and $P_k$ along the cable and $\omega$ denotes the circular frequency, neglecting the imaginary part ($q$-spectrum), the CPSD function of $\tilde{W}(x_j,t)$ and $\tilde{W}(x_k,t)$ can be expressed as follows:

$$S_{\tilde{W}_j\tilde{W}_k}(x_j, x_k; \omega) = S_{\tilde{W}\tilde{W}}(\omega)\mathrm{Coh}_{\tilde{W}}(v_{jk}, \omega) \tag{9}$$

In Eq. (9) $S_{\tilde{W}\tilde{W}}(\omega) \equiv S_{\tilde{W}_j\tilde{W}_j}(x_j, x_j; \omega)$ is the PSD function of $\tilde{W}(x,t)$ for $x_j \equiv x_k$, which is assumed constant over the spatial domain $[0,l]$, as usual for extended horizontal structures under wind action. Since in the present context, the random field $\tilde{W}(x,t)$ is isotropic, i.e., its autocorrelation function depends only upon the absolute value of the separation distance $v_{jk}=|\mu_{jk}|=|x_k-x_j|$ between two point locations $P_j$ and $P_k$, the coherence function $\mathrm{Coh}_{\tilde{W}}(v_{jk}, \omega)$ is defined according to Davenport model (1968), as follows:

$$\mathrm{Coh}_{\tilde{W}}(v_{jk}, \omega) = \exp[-\alpha(\omega)v_{jk}]; \quad \alpha(\omega) = \frac{|\omega|}{2\pi}\frac{C_x}{\overline{W}(h)} \tag{10}$$

where $C_x$ is an appropriate exponential decay coefficient.

It has to be mentioned that the stochastic model of natural wind above defined is referred to shallow cables, which may be reasonably regarded as horizontal string-like exposed structures. To cover also deep-sag cables, the present formulation should duly account for the variability of the PSD function over the spatial domain $[0, l]$, caused by the change of the mean wind velocity along cable profile. Furthermore, a consistent definition of the coherence function should be assumed.

The aerodynamic forces are determined referring to a spring-mounted damped rigid cylinder of indefinite length with two translational degrees-of-freedom subjected to the mean wind velocity $\overline{W}(h)$ and the longitudinal zero-mean fluctuation $\tilde{W}(x, t)$, in the quasi-static regime (i.e., at much lower oscillation frequencies than the vortex-shedding frequency (Simiu and Scanlan 1996)), (Piccardo 1993). Numerical experience has shown that the first and second-order statistical moments of cable response are weakly influenced by the nonlinear aerodynamic terms. Since the proposed procedure is aimed at second-order analysis of wind-induced cable vibrations, such terms are here neglected to enhance the computational efficiency. It is worth noting, however, that the present formulation can be properly extended to include nonlinear aerodynamic contributions as well. Under the previous hypotheses and assuming small turbulence with respect to the mean wind velocity, the linearized expressions of the drag force components acting on a cable of circular cross-section along the $y$ and $z$ axes read, respectively (Pasca, *et al.* 1998):

$$f_y(x, t) = -\frac{1}{2}\rho C_D b\overline{W}(h)\dot{v}(x, t) \tag{11}$$

$$f_z(x, t) = \frac{1}{2}\rho C_D b\overline{W}^2(h) - \rho C_D b\overline{W}(h)\dot{w}(x, t) + \rho C_D b\overline{W}(h)\tilde{W}(x, t) \tag{12}$$

where $\rho$ is the air density, $C_D$ is the drag coefficient and $b$ denotes a characteristic dimension of the body, which in the present case coincides with cable diameter (indefinite circular cylinder). Notice that the drag force component in the across-wind direction $f_y(x, t)$ (Eq. (11)) provides just a positive aerodynamic damping contribution, so that in-plane vibrations are only indirectly excited through the nonlinear coupling terms. Conversely, in the along-wind direction, beside a linear aerodynamic damping, the blowing wind induces two external excitations, a constant $(\rho C_D b\overline{W}^2(h)/2)$ and a time-varying one $(\rho C_D b\overline{W}(h)\tilde{W}(x, t))$, associated with the mean and fluctuation of wind velocity, respectively. Owing to the random nature of wind turbulence, the time-varying term gives rise to a stochastic dynamic excitation.

## 3. Monte Carlo-based analysis of wind-induced nonlinear cable vibrations

In view of the nonlinearity of the equations governing cable motion (see Eqs. (6)-(7)), Monte Carlo simulation (MCS) method is here selected as an effective tool for the probabilistic characterization of wind-induced random vibrations in terms of first and second-order statistical moments. According to Double Modal Transformation (DMT) approach (Carassale, *et al.* 2001), the time-domain analysis of buffeting response is carried out through the joint application of Galerkin's method and the Proper Orthogonal Decomposition (POD) of wind turbulence field. So operating, a computationally efficient technique for digital simulation of the generalized aerodynamic loads is developed, as will be outlined in the following.

### *3.1. Galerkin's discretization of the equations of motion*

The time-domain analysis of cable response to the aerodynamic loads defined in the previous section is here performed by assuming the following expressions of the transversal displacement components $v(x,t)$ and $w(x,t)$:

$$v(x,t) = \sum_{i=1}^{n_v} \varphi_i(x) q_i(t); \qquad w(x,t) = \sum_{k=1}^{n_w} \psi_k(x) r_k(t) \tag{13}$$

where $\varphi_i(x)$ and $\psi_k(x)$ are the in-plane and out-of-plane (or swinging) eigenfunctions of the associated linear problem obtained dropping all the nonlinear terms in Eqs. (6) and (7) (see Appendix A). Hereinafter, therefore, $\varphi_i(x)$ and $\psi_k(x)$ will be referred to as linearized eigenfunctions; $q_i(t)$ and $r_k(t)$ are the corresponding generalized coordinates.

Substituting the previous relations into Eq. (5), an approximate expression of the time-varying elongation $\varepsilon^{(c)}(t)$ is recovered:

$$\hat{\varepsilon}^{(c)}(t) = \sum_{j=1}^{n_v} b_j^{(1)} q_j(t) + \sum_{i,j=1}^{n_v} b_{ij}^{(2)} q_i(t) q_j(t) + \sum_{k=1}^{n_w} b_k^{(3)} r_k^2(t) \tag{14}$$

where the superimposed hat (^) means that use has been made of the series expansions (13); $b_j^{(1)}$, $b_{ij}^{(2)}$ and $b_k^{(3)}$ are coefficients defined in Appendix B. By applying Galerkin's method and taking into account Eq. (14), the partial integro-differential Eqs. (6) and (7) are replaced by the following set of $n_v+n_w$ nonlinear coupled ordinary differential equations in the generalized coordinates $q_i(t)$ and $r_k(t)$:

$$\ddot{q}_i(t) + \hat{\mu}_{vi}\dot{q}_i(t) + \sum_{j=1}^{n_v} a_{ij}^{(1)} q_j(t) + \left[ a_i^{(2)} + \sum_{j=1}^{n_v} a_{ij}^{(3)} q_j(t) \right] \hat{\varepsilon}^{(c)}(t) = 0, \qquad (i = 1, 2, ..., n_v); \tag{15}$$

$$\ddot{r}_k(t) + \hat{\mu}_{wk}\dot{r}_k(t) + \omega_{wk}^2 r_k(t) + a_k^{(4)} \hat{\varepsilon}^{(c)}(t) r_k(t) = \bar{F}_{zk} + \tilde{F}_{zk}(t), \qquad (k = 1, 2, ..., n_w) \tag{16}$$

where $\hat{\mu}_{vi}$ and $\hat{\mu}_{wk}$ are modal damping coefficients including the positive contribution due to linear aerodynamic damping (see Appendix B); $\omega_{wk}$ denotes the natural frequency of the $k$-th out-of-plane mode for the associated linear problem (see Appendix A); $a_{ij}^{(1)}$, $a_i^{(2)}$, $a_{ij}^{(3)}$ and $a_k^{(4)}$ are coefficients whose expressions, listed in Appendix B, depend on both cable parameters and the selected mode shapes. Furthermore, the generalized force on the right-hand side of the $k$-th out-of-plane modal Eq. (16)

is expressed as sum of a constant load of deterministic nature, $\bar{F}_{zk}$, associated with the mean wind velocity, and a stochastic time-varying excitation, $\tilde{F}_{zk}(t)$, related to wind turbulence:

$$\bar{F}_{zk} = \frac{1}{2}\rho C_D b F_{zk}^{(1)} \bar{W}^2(h) \tag{17}$$

$$\tilde{F}_{zk}(t) = \rho C_D b F_{zk}^{(2)} \bar{W}(h) \int_0^l \psi_k(x) \tilde{W}(x, t) \mathrm{d}x \tag{18}$$

where $F_{zk}^{(1)}$ and $F_{zk}^{(2)}$ are coefficients defined in Appendix B.

### *3.2. Proper Orthogonal Decomposition of wind velocity fluctuation*

Embedding the above defined Galerkin-type discretized model into a Monte Carlo framework requires the digital simulation of the fluctuating generalized drag forces $\tilde{F}_{zk}(t)$ (Eq. (18)), which is here performed by properly extending a procedure recently proposed for multivariate 1D random processes (Di Paola 1998, Di Paola and Gullo 2001). This technique starts by decomposing the 1V-2D stationary zero-mean Gaussian random field, $\tilde{W}(x, t)$, modeling wind turbulence in the spatial domain $[0, l]$, as a summation of fully coherent independent stochastic fields (Li and Kareem 1993), according to the POD (Loeve 1955, Papoulis 1965):

$$\tilde{W}(x, t) = \sum_{r=1}^{\infty} \tilde{V}_r(x, t) \tag{19}$$

The previous representation is not unique as the definition of the random fields $\tilde{V}_r(x, t)$ depends on the way in which the CPSD function of wind velocity fluctuation $\tilde{W}(x, t)$ is decomposed. Within a discrete setting, in Refs. (Di Paola 1998, Di Paola and Gullo 2001), the decomposition of the CPSD matrix into the frequency-dependent basis of its eigenvectors has been adopted, emphasizing the physical meanings and the computational advantages connected with this particular choice. In a similar way, since, by definition, the CPSD function is bounded, symmetric and positive-definite, the following spectral decomposition is here exploited for digital simulation purposes:

$$S_{\tilde{W}_j \tilde{W}_k}(x_j, x_k; \omega) = \sum_{p=1}^{\infty} \lambda_p(\omega) \phi_p(x_j, \omega) \phi_p(x_k, \omega) \tag{20}$$

where $\lambda_p(\omega)$ and $\phi_p(x, \omega)$ denote the frequency-dependent eigenvalues and eigenfunctions of the CPSD function, respectively. It can be verified that, if $S_{\tilde{W}_j \tilde{W}_k}(x_j, x_k; \omega)$ is decomposed according to Eq. (20), the Priestley (1999) representation of the random fields $\tilde{V}_r(x, t)$ takes the following expression:

$$\tilde{V}_r(x, t) = \int_{-\infty}^{+\infty} \sqrt{\lambda_r(\omega)} \phi_r(x, \omega) e^{i\omega t} \mathrm{d}B_r(\omega) \tag{21}$$

$i$ being the imaginary unit and $B_r(\omega)$ a zero-mean normal complex random process having orthogonal increments, i.e.:

$$E[\mathrm{d}B_r(\omega)] = 0; \quad \mathrm{d}B_r(\omega) = \mathrm{d}B_r^*(-\omega); \quad E[\mathrm{d}B_r(\omega_m)\mathrm{d}B_s^*(\omega_n)] = \delta_{rs}\delta_{mn}\mathrm{d}\omega_m \tag{22}$$

where $E[\cdot]$ and the star mean stochastic average and complex conjugate, respectively; $\delta_{rs}$ is the Kronecker delta symbol ($\delta_{rs}=0$, $r \neq s$; $\delta_{rs}=1$, $r=s$). Indeed, the autocorrelation function of the random field $\tilde{W}(w, t)$ decomposed as in Eq. (19) with $\tilde{V}_r(x, t)$ expressed by Eq. (21) coincides with the Inverse Fourier Transform of the CPSD function (20):

$$R_{\tilde{W}_j\tilde{W}_k}(\mu_{jk}, \tau) = E[\tilde{W}(x_k, t+\tau)\tilde{W}^*(x_j, t)] = \sum_{r=1}^{\infty}\int_{-\infty}^{+\infty}\lambda_r(\omega)\phi_r(x_j, \omega)\phi_r(x_k, \omega)e^{i\omega\tau}\mathrm{d}\omega \tag{23}$$

Sorting the eigenvalues $\lambda_p(\omega)$ in decreasing order and taking into account that only the first few spectral modes, say $M$, exhibit a significant power, the random field $\tilde{W}(x, t)$ can be expressed by means of the following truncated series expansion:

$$\tilde{W}(x, t) = \sum_{r=1}^{M}\tilde{V}_r(t) = \sum_{r=1}^{M}\int_{-\infty}^{+\infty}\sqrt{\lambda_r(\omega)}\phi_r(x, \omega)e^{i\omega t}\mathrm{d}B_r(\omega) \tag{24}$$

If the circular frequency domain is uniformly discretized, the previous relation may be employed to digitally generate wind velocity time-histories at selected point locations.

The eigenproperties of the CPSD function, exploited in the above described orthogonal decomposition of wind turbulence field, are the non-trivial solutions of the following Fredholm integral equation of the second kind:

$$\int_0^l S_{\tilde{W}_j\tilde{W}_k}(x_j, x_k; \omega)\phi_p(x_j, \omega)\mathrm{d}x_j = \lambda_p(\omega)\phi_p(x_k, \omega) \tag{25}$$

which, substituting Eqs. (9) and (10), may be rewritten as:

$$S_{\tilde{W}\tilde{W}}(\omega)\int_0^l \exp[-\alpha(\omega)|x_k - x_j|]\phi_p(x_j, \omega)\mathrm{d}x_j = \lambda_p(\omega)\phi_p(x_k, \omega) \tag{26}$$

Since the CPSD function (9) is real, symmetric and positive-definite, it possesses real and non-negative eigenvalues $\lambda_p(\omega)$; the eigenfunctions $\phi_p(x, \omega)$ are real, form a complete set and can be normalized so as to satisfy the following condition:

$$\int_0^l \phi_p(x, \omega)\phi_q(x, \omega)\mathrm{d}x = \delta_{pq}, \quad \forall\omega \tag{27}$$

It can be verified that the eigenfunctions and eigenvalues solutions of Eq. (26) read, respectively (Carassale and Solari 2002):

$$\phi_p(x,\omega) = C_p\left\{\sin[\beta_p(\omega)x] + \frac{\beta_p(\omega)}{\alpha(\omega)}\cos[\beta_p(\omega)x]\right\}; \quad \lambda_p(\omega) = \frac{2S_{\tilde{W}\tilde{W}}(\omega)\alpha(\omega)}{\beta_p^2(\omega)+\alpha^2(\omega)} \tag{28}$$

where $C_p$ are constants defined imposing the normalization condition (27), while $\beta_p(\omega)$ are the roots of the following trascendental equation:

$$2\cot[l\beta_p(\omega)] = \frac{\beta_p(\omega)}{\alpha(\omega)} - \frac{\alpha(\omega)}{\beta_p(\omega)} \tag{29}$$

The solution of Eq. (26) may be found also in Refs. (Van Trees 1968, Spanos and Ghanem 1989), where different expressions for odd and even eigenproperties are given. Likewise out-of-plane linearized mode shapes of a suspended cable, odd and even eigenfunctions are symmetric and antisymmetric about cable mid-span, respectively. Furthermore, it is worth noting that the eigenfunctions depend only indirectly upon circular frequency $\omega$ through the functions $\beta_p(\omega)$.

The main drawback of the previous POD of the random field $\tilde{W}(x,t)$ consists in the evaluation of the frequency-dependent eigenproperties of the CPSD function, which implies the numerical solution of the trascendental Eq. (29) at each frequency step. In this regard, it would be desirable to know analytic expressions of the solutions of the eigenproblem (26), like the approximate ones derived in Ref. (Carassale and Solari 2002). Though their evaluation may be time-consuming, the eigenproperties of the CPSD function lend themselves to a meaningful physical interpretation, which enlightens the mutual interaction between wind loading and structural vibrations within the framework of mode-superposition analysis. It appears, in fact, that the eigenvalues and eigenfunctions may be regarded as the powers of the random fields $\tilde{V}_r(x,t)$ (see Eq. (21)) and the mode shapes associated with wind velocity field, respectively. Therefore, Eq. (24) suggests an analogy between the above described representation of wind velocity fluctuation $\tilde{W}(x,t)$ and classical modal analysis. Specifically, as a structural vibration is decomposed into a series of independent structural mode shapes, in the same way, the 1V-2D random field $\tilde{W}(x,t)$ is expressed as summation of a sufficient number of fully coherent uncorrelated fields which, therefore, can be called *blowing modes* of wind velocity field.

### 3.3. Digital simulation of the generalized aerodynamic loads

As far as digital simulation of the aerodynamic loads on a wind-excited suspended cable is concerned, the previous orthogonal decomposition of the random field $\tilde{W}(x,t)$ (see Eq. (24)) in conjunction with Galerkin's discretization of the motion equations (see Eqs. (15) and (16)), provides substantial computational savings, mainly related to the above discussed physical interpretation. In this connection, let us substitute Eq. (24) into Eq. (18), so that the fluctuating component of the generalized aerodynamic loads $\tilde{F}_{zk}(t)$ can be expressed as follows:

$$\tilde{F}_{zk}(t) = \rho C_D b F_{zk}^{(2)}\overline{W}(h)\sum_{r=1}^{M}\int_{-\infty}^{+\infty}\sqrt{\lambda_r(\omega)}D_{kr}(\omega)e^{i\omega t}\mathrm{d}B_r(\omega), \quad (k=1,2,...,n_w) \tag{30}$$

where:

$$D_{kr}(\omega) = \int_0^l \psi_k(x)\phi_r(x,\omega)\mathrm{d}x \tag{31}$$

are functions of the circular frequency $\omega$, obtained by projecting the $r$-th blowing mode shape on the $k$-th out-of-plane linearized eigenfunction of the cable. Subdividing the frequency range into intervals of equal amplitude $\Delta\omega$, Eq. (30) can be rewritten in the following discretized form, useful for digital simulation purposes:

$$\tilde{F}_{zk}(t) = \rho C_D b F_{zk}^{(2)} \overline{W}(h) \sum_{r=1}^{M} \sum_{n=-N}^{N} \sqrt{\lambda_r(\omega_n)\Delta\omega} D_{kr}(\omega_n) e^{i\omega_n t} P_n^{(r)}, \quad (k = 1, 2, ..., n_w) \tag{32}$$

where $\omega_n = n\Delta\omega$, $N\Delta\omega = \omega_c$ is the upper cut-off frequency and $P_n^{(r)}$ denote mutually independent zero-mean normal complex random variables with unit variance, i.e.:

$$E[P_n^{(r)}] = 0;\ E[P_n^{(r)} P_m^{(s)^*}] = \delta_{rs}\delta_{nm};\ P_n^{(r)} = P_{-n}^{(r)^*} \tag{33}$$

Alternatively, Eq. (32) may be rewritten in real form as follows:

$$\tilde{F}_{zk}(t) = \rho C_D b F_{zk}^{(2)} \overline{W}(h) \sum_{r=1}^{M} \sum_{n=-N}^{N} \sqrt{\lambda_r(\omega_n)\Delta\omega} D_{kr}(\omega_n)[R_n^{(r)}\cos(\omega_n t) - I_n^{(r)}\sin(\omega_n t)], \quad (k=1,2,...,n_w) \tag{34}$$

where $R_n^{(r)}$ and $I_n^{(r)}$ are mutually independent zero-mean normal random variables with variance 1/2, representing the real and imaginary part of $P_n^{(r)}$, respectively, that is $P_n^{(r)} = R_n^{(r)} + iI_n^{(r)}$.

The shapes of the eigenfunctions $\psi_k(x)$ (see Appendix A) and $\phi_r(x,\omega)$ (Eq. (28)) are such that for $k$ odd (symmetric out-of-plane cable mode shape) and $r$ even (antisymmetric blowing mode shape), or vice-versa, the integrals $D_{kr}(\omega)$ (Eq. (31)) vanish identically, since structural and wind modes are orthogonal. Furthermore, numerical investigations have shown that when $k$ and $r$ are both odd or even the contributions of the integrals $D_{kr}(\omega)$ with different indices ($r \neq k$) are almost negligible, namely $\psi_k(x)$ and $\phi_r(x,\omega)$ are quasi-orthogonal. Since the functions $D_{kr}(\omega)$, ($r=1,2,...,M$), may be regarded as a measure of the influence of the first $M$ blowing modes on the $k$-th cable swinging mode, physically this means that the $k$-th out-of-plane structural mode is actually dominated just by the $k$-th wind mode. It follows that at least $n_w$ blowing modes should be considered to simulate the first $n_w$ random loads $\tilde{F}_{zk}(t)$. Moreover, it has been observed that the functions $D_{kr}(\omega)$ are nearly constant except in a very small low-frequency range, as will be shown next through numerical results. In view of these interesting properties, the computational efficiency of the digital simulation technique based on the use of Eq. (34) may be greatly enhanced by means of the following assumptions: i) only the terms related to the functions $D_{kk}(\omega)$ with equal indices ($r=k$) are retained in the summation; ii) over the whole frequency range each function $D_{kk}(\omega)$ is given the constant value $D_{kk}(\omega_c)$, corresponding to the upper cut-off frequency $\omega_c$. According to these hypotheses, Eq. (34) may be conveniently simplified setting $D_{kr}(\omega)=0$ for $r \neq k$ and $D_{kk}(\omega)=D_{kk}(\omega_c)=const$, i.e.:

$$\tilde{F}_{zk}(t) = \rho C_D b F_{zk}^{(2)} \overline{W}(h) D_{kk}(\omega_c) \sum_{n=-N}^{N} \sqrt{\lambda_k(\omega_n)\Delta\omega} [R_n^{(k)}\cos(\omega_n t) - I_n^{(k)}\sin(\omega_n t)], \quad (k=1,2,...,n_w) \tag{35}$$

The previous relation ensures a drastic reduction of the computer time required by digital simulation of the random processes $\tilde{F}_{zk}(t)$. The main advantages associated with the use of Eq. (35) may be summarized as follows: i) it is required the evaluation of very few eigenproperties of the CPSD function, say $n_w$, as many as are the out-of-plane linearized mode shapes of the cable included in Eq. (13); ii) the integrals $D_{kk}(\omega)$ (Eq. (31)) and, therefore, the eigenfunctions $\phi_k(x, \omega)$ need to be calculated only for $\omega=\omega_c$; iii) the onerous evaluation of the double summation appearing in Eq. (34) is avoided.

It can be easily demonstrated that the $k$-th fluctuating load $\tilde{F}_{zk}(t)$, defined by Eq. (30), is a 1V-1D random process, whose PSD function, $S_{\tilde{F}_{zk}}(\omega)$, is proportional to the $k$-th eigenvalue $\lambda_k(\omega)$ of $S_{\tilde{W}_j\tilde{W}_k}(x_j, x_k; \omega)$, i.e.:

$$S_{\tilde{F}_{zk}}(\omega) = (\rho C_D b F_{zk}^{(2)} \overline{W}(h) D_{kk}(\omega_c))^2 \lambda_k(\omega), \quad (k = 1, 2, ..., n_w) \tag{36}$$

Hence, once the first $n_w$ eigenproperties of the CPSD function of wind turbulence field $\tilde{W}(x, t)$ are known, digital simulation of the aerodynamic forces acting on the suspended cable may be performed through conventional wave-superposition-based procedures commonly employed for 1V-1D random processes with given spectral distribution (see Eq. (35)). So operating, the present procedure is able to model the cross-correlation between wind velocity fluctuations at different point locations more efficiently than widely used approaches based on the spatial discretization of wind turbulence field into an $n$V-1D stochastic process, $n$ being the number of the selected simulation points. In particular, conventional spectral methods for digital simulation of stationary Gaussian multivariate random processes require the repetitive factorization of the CPSD matrix at each frequency step, which is usually performed by Cholesky decomposition. It can be verified that, if the CPSD matrix is decomposed as the product of two frequency-dependent triangular matrices, the computer time for the generation of an $n$V-1D random process increases with the law $n(n+1)/2$, becoming actually prohibitive when a large number of variates is involved. Therefore, the main drawback of these procedures lies in the severe limitations imposed on the number of simulation points.

Based on the previous observations, it may be stated that the proposed simulation algorithm allows one to carry out a Monte Carlo-based analysis of wind-induced cable vibrations with a quite reasonable computational effort. The following steps are involved in implementing the overall procedure:

1) evaluation of the first $n_w$ eigenvalues $\lambda_r(\omega)$ of $S_{\tilde{W}_j\tilde{W}_k}(x_j, x_k; \omega)$, with $\omega$ ranging over the interval $[0, \omega_c]$, and of the corresponding eigenfunctions $\phi_r(x, \omega)$ just for $\omega=\omega_c$;
2) calculation of the integrals $D_{kk}(\omega)$, $(k=1,2, ..., n_w)$, for $\omega=\omega_c$;
3) digital simulation of samples of the random processes $\tilde{F}_{zk}(t)$, $(k=1,2,...,n_w)$ through Eq. (35);
4) evaluation of response time-histories by numerical integration of Eqs. (15) and (16);
5) processing of response samples to obtain the desired statistics.

## 4. Numerical applications

In this section, the effectiveness of the proposed procedure for analyzing wind-induced cable vibrations is demonstrated by examining two different cables, referred to as cable N°1 and N°2. The main geometrical and mechanical properties of cable N°1 are defined as follows: $l=266.984$ m, $d/1=1/45$, $EA/H=486$, $m=1.8$ kg/m and $b=2.81 \cdot 10^{-2}$ m. The same properties for cable N°2 are given by: $l$=850 m, $d/l$=1/25, $EA/H$=735.257, $m$=2.52 kg/m and $b$=3.58 · $10^{-2}$ m. The elasto-geometric parameter $\lambda^2=64(EA/H)(d/l)^2$ (Irvine 1981), governing cable dynamics (see Appendix A), takes the value $\lambda^2$=15.36, on the left of the first crossover point ($\lambda^2=4\pi^2$), for cable N°1 and $\lambda^2$=75.29, between the first and second ($\lambda^2=16\pi^2$) crossover point, for cable N°2 (see Fig. 11). In Table 1 the first four in-plane and out-of-plane linearized mode shapes of the two cables along with the corresponding natural frequencies are reported.

The mean wind velocity is here assumed to vary as a function of the height $h$ above ground, according to the well known logarithmic profile:

$$\overline{W}(h) = \frac{u_*}{k}\ln\left(\frac{h}{z_0}\right) \tag{37}$$

where $u_*$[m/s] is the shear velocity, $k$=0.4 is the Von Karman's constant and $z_0$ [m] is the roughness length. The two-sided PSD function of wind velocity fluctuation proposed by Kaimal *et al.* (1972) is adopted:

$$S_{\tilde{W}\tilde{W}}(\omega) = \frac{1}{4\pi}200u_*^2\frac{h}{\overline{W}(h)}\frac{1}{\left(1+50\dfrac{|\omega|h}{2\pi\overline{W}(h)}\right)^{5/3}} \tag{38}$$

The parameters characterizing wind velocity field and the ensuing aerodynamic loads are selected as follows: $\overline{W}(h)$=25 m/s, $\rho$=1.25 kg/m$^3$, $C_D$=1, $C_x$=16 (see Eq. (10)), $z_0$=0.01 m, $h$=20 m for cable N°1 and $h$=50 m for cable N°2. The upper cut-off frequency $\omega_c$ is set equal to 6 rad/s. Moreover, the modal damping ratios are assumed equal for all modes, setting $\zeta_v=\zeta_{vi}$=0.004 and $\zeta_w=\zeta_{wk}$=0.001 for both cable N°1 and N°2 (see Appendix B). Newmark-$\beta$ method ($\beta$=1/4, $\gamma$=1/2) associated with full Newton-Raphson iterative procedure is applied to integrate the nonlinear ordinary differential Eqs. (15) and (16) ruling cable response in the generalized space.

Before examining the computational and physical aspects connected with the analysis of cable vibrations by the proposed procedure, the main features of the spectral decomposition of the CPSD function of wind velocity fluctuation are briefly outlined (see Eq. (20)). For this purpose, some numerical results concerning the representation of wind turbulence field on cable N°1 are presented. In Fig. 2 the first six eigenvalues $\lambda_p(\omega)$ of $S_{\tilde{W}_j\tilde{W}_k}(x_j, x_k; \omega)$ versus frequency are plotted. Notice that in the low-frequency range the first eigenvalue dominates the other ones, while for higher values of $\omega$ all the eigenvalues tend to the same value. Physically, this means that for low frequencies the first blowing modes exhibit the major power content so that they represent almost completely the random field $\tilde{W}(x, t)$. In Fig. 3 the first six eigenfunctions $\phi_p(x,\omega)$ of $S_{\tilde{W}_j\tilde{W}_k}(x_j, x_k; \omega)$ for different

Table 1 First four in-plane and out-of-plane linearized mode shapes and natural frequencies (Cables N°1 and N°2)

| Cable N°1 ($\lambda^2<4\pi^2$) | | | | | | Cable N°2 ($4\pi^2<\lambda^2<16\pi^2$) | | | | | |
|---|---|---|---|---|---|---|---|---|---|---|---|
| In-plane | | $\omega_v$[rad/s] | Out-of-plane | | $\omega_w$[rad/s] | In-plane | | $\omega_v$[rad/s] | Out-of-plane | | $\omega_w$[rad/s] |
| 1° | Sym. | 2.1338 | 1° | Sym. | 1.4282 | 1° | Antisym. | 1.1932 | 1° | Sym. | 0.5966 |
| 2° | Antisym. | 2.8565 | 2° | Antisym. | 2.8565 | 2° | Sym. | 1.4574 | 2° | Antisym. | 1.1932 |
| 3° | Sym. | 4.3238 | 3° | Sym. | 4.2847 | 3° | Sym. | 1.9574 | 3° | Sym. | 1.7899 |
| 4° | Antisym | 5.7129 | 4° | Antisym | 5.7129 | 4° | Antisym. | 2.3865 | 4° | Antisym | 2.3865 |

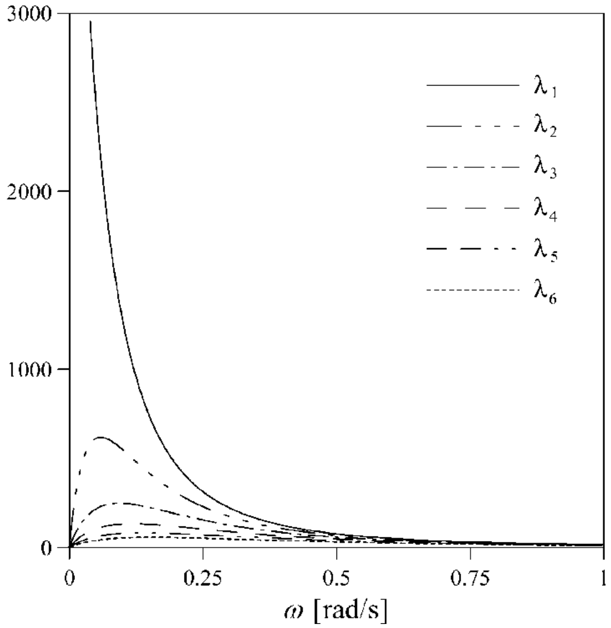


Fig. 2 First six eigenvalues of the CPSD function versus frequency $\omega$ (cable N°1)

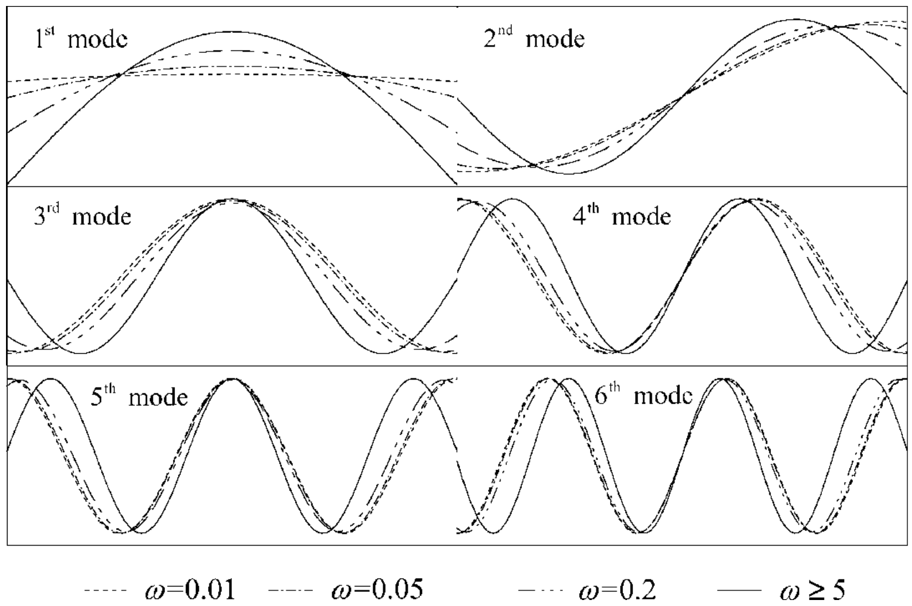


Fig. 3 First six blowing mode shapes for different values of frequency $\omega$ (cable N°1)

values of frequency are shown. It can be seen that the blowing mode shapes vary appreciably in the low frequency range, while after a certain value of $\omega$ they remain practically unchanged. As already mentioned, the eigenfunctions $\phi_p(x,\omega)$ indeed depend only indirectly upon frequency through the functions $\beta_p(\omega)$ (see Eq. (28)), which are nearly constant except for low frequencies (Di Paola, *et al*.

2002). Furthermore, it is interesting to underline the similarity between the blowing mode shapes and the corresponding out-of-plane linearized eigenfunctions of the suspended cable. As will be shown next, the aforementioned similarity actually represents the core of the proposed simulation algorithm. In Fig. 4 the convergence of the eigenfunction expansion of the PSD and CPSD functions to the target spectra is illustrated for $x_j=x_k=l/2$ and $x_j=l/4$, $x_k=l/2$, respectively. Notice that in both cases few eigenproperties are enough to obtain a satisfactory match with the target spectrum, though for the PSD function (Fig. 4a) the convergence is rather slower.

Let us now focus our attention on the time-domain analysis of cable response under wind loading. For a better understanding of the simplifications introduced in Eq. (35), in Fig. 5 the functions $D_{kr}(\omega)$ (Eq. (31)) associated with the first four out-of-plane linearized eigenfunctions $\psi_k(x)$, ($k$=1,2,...,4), of cable N°1 and the first six wind mode shapes $\phi_r(x,\omega)$, ($r$=1,2,...,6), are plotted. It clearly appears that the contribution of the cross terms, i.e., $D_{kr}(\omega)$ with $r \neq k$, can be reasonably neglected. Moreover, the frequency dependence of the functions $D_{kk}(\omega)$ with equal indices can be disregarded as well, assuming for convenience $D_{kk}(\omega)=D_{kk}(\omega_c)$. In Fig. 6a the legitimacy of the above discussed assumptions concerning the integrals $D_{kr}(\omega)$ is demonstrated through an appropriate comparison between samples of the random process $\tilde{F}_{z1}(t)$ generated by Eq. (34) and Eq. (35) (for $k$=1). Fig. 6b displays an analogous comparison between the corresponding samples of mid-span out-of-plane vibrations of cable N°1, computed assuming $n_v=n_w=M=4$. It appears that Eq. (34) can be conveniently replaced by Eq. (35) for digital simulation purposes, without affecting remarkably the accuracy of results.

A crucial aspect to be investigated is represented by the suitable number of wind ($M$) and cable modes ($n_v$ and $n_w$) to be included in the analysis. Numerical experience has revealed that the number of blowing modes affecting cable vibrations is less than the one required to accurately

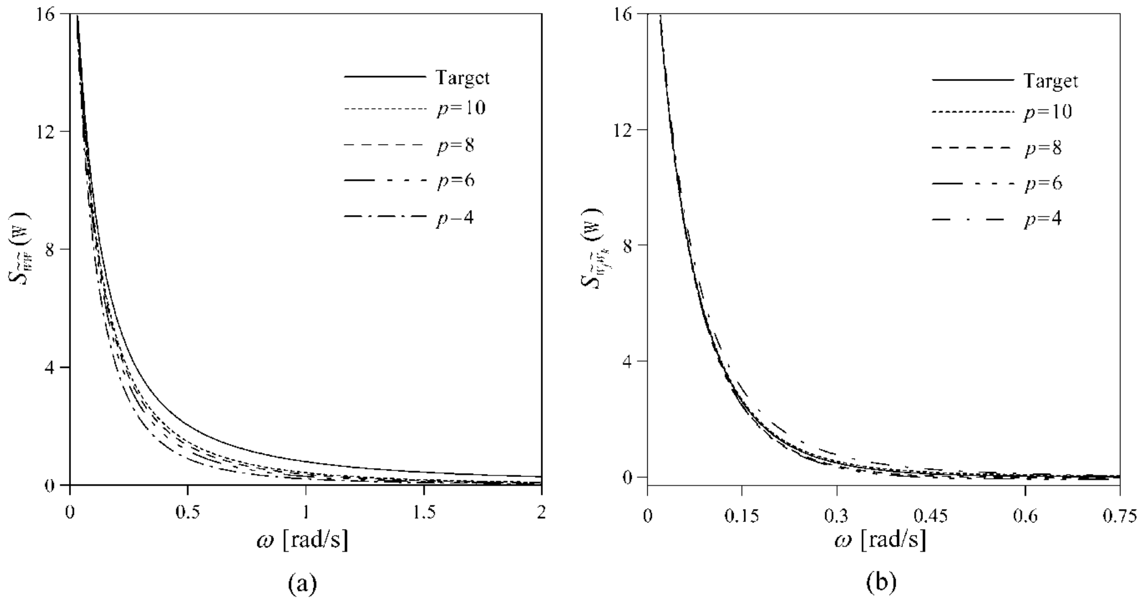


Fig. 4 Comparison between target power spectrum of wind velocity fluctuation and eigenfunction expansion for an increasing number $p$ of spectral modes (Eq. (20)): (a) $x_j=x_k=l/2$; (b) $x_j=l/4$ and $x_k=l/2$ (cable N°1)

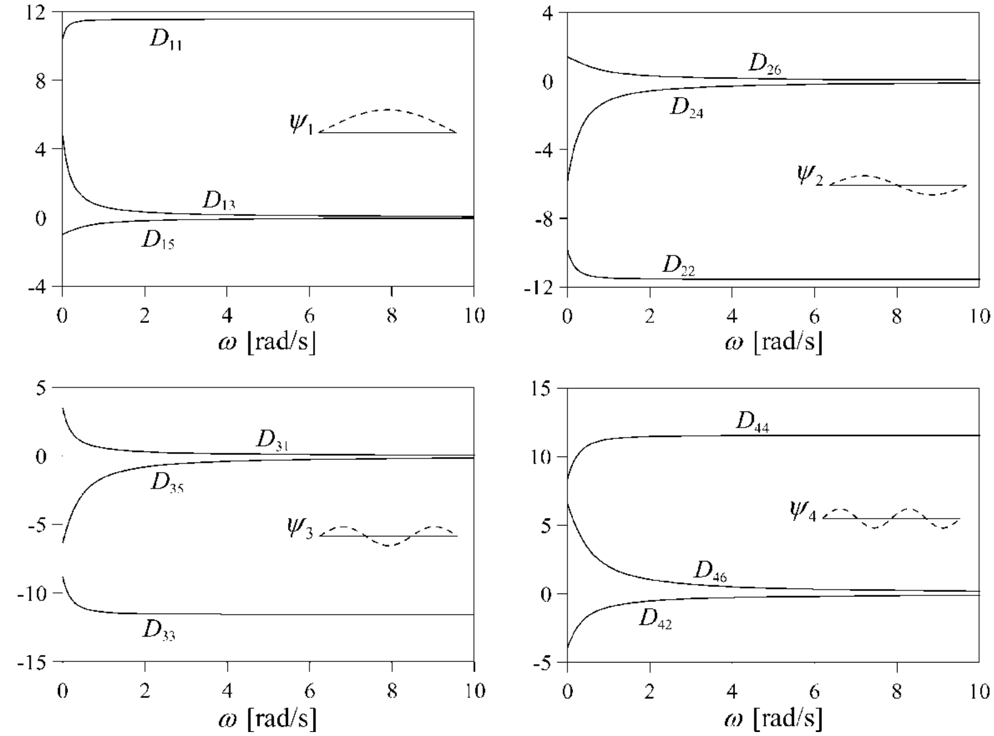


Fig. 5 Functions $D_{kr}(\omega)$ versus frequency $\omega$, for $k$=1,2,..., 4 and $r$=1,2,...,6 (cable N°1)

represent wind turbulence field over the spatial domain [0, $l$]. Specifically, it has been observed that samples of cable response may be adequately predicted considering just the first $n_w$ wind modes according to Eq. (35). On the other hand, the appropriate order of the Galerkin-type discretized model, obtained approximating the transversal displacement components through Eq. (13), is dictated by the geometrical and mechanical properties of the cable (Irvine parameter $\lambda^2$) as well as by the phenomena to be investigated within the framework of nonlinear dynamic behavior. In Fig. 7 samples of out-of-plane vibrations of cables N°1 and N°2 at $x=l/4$, obtained including one to three structural and wind modes, are plotted. Notice that a two-degree-of-freedom discretized model ($n_v=n_w=M=1$) seems satisfactory for cable N°1, whose first in-plane eigenfunction is symmetric (see Table 1). Conversely, such a model is quite inadequate to predict the response of cable N°2, since its first in-plane mode is antisymmetric and therefore is not excited by the first wind mode. In fact, in that case the nonlinear coupling terms appearing in Eq. (15) vanish identically and a pure swinging motion of the cable is devised. It follows that at least the first two structural (in-plane and out-of-plane) and loading modes ($n_v=n_w=M=2$) should be included to allow for the vertical vibrations to be excited. Nevertheless, further investigations reveal that a two-degree-of-freedom discretized model is always inaccurate, even for cables on the left of the first crossover point, since it is unable to capture the loss of coherence induced in the response process by the spatially correlated wind turbulence. Indeed, including only one blowing mode ($M=1$) in the orthogonal decomposition (24) means assuming that wind velocity field is fully coherent. The previous concept is exhaustively illustrated in Figs. 8 and 9. Fig. 8 shows samples of out-of-plane vibrations of cable N°1 at $x_j=l/4$ and $x_k=3l/4$ ($v_{jk}$=133.492 m) evaluated assuming both $n_v=n_w=M=1$ (Fig. 8a) and

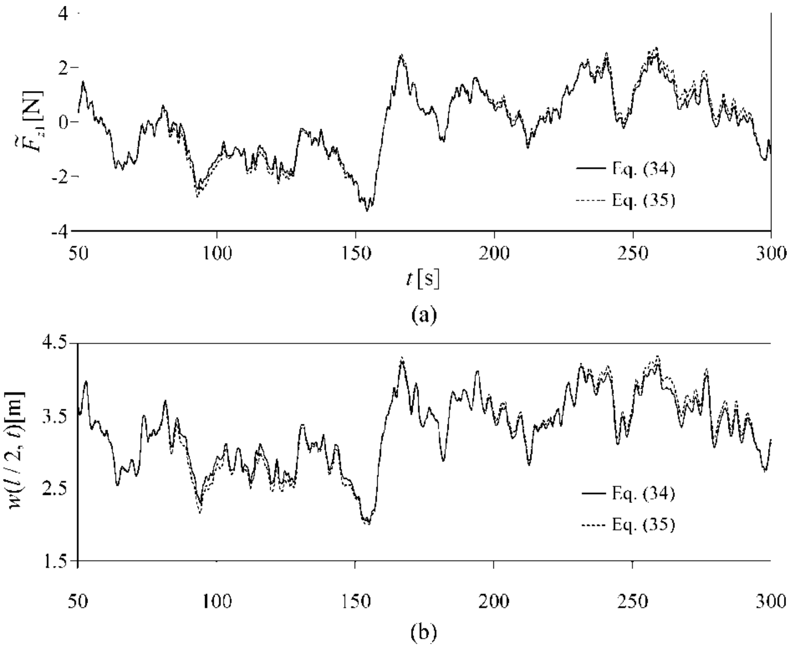


Fig. 6 Comparison between samples of $\tilde{F}_{z1}(t)$ simulated through Eq. (34) and Eq. (35) for cable N$^{o}$ 1 (a). Comparison between samples of mid-span out-of-plane response of cable N$^{o}$1 to the generalized loads $\tilde{F}_{zk}(t)$, ($k$=1,2,...,4), simulated through Eq. (34) and Eq. (35) (b)

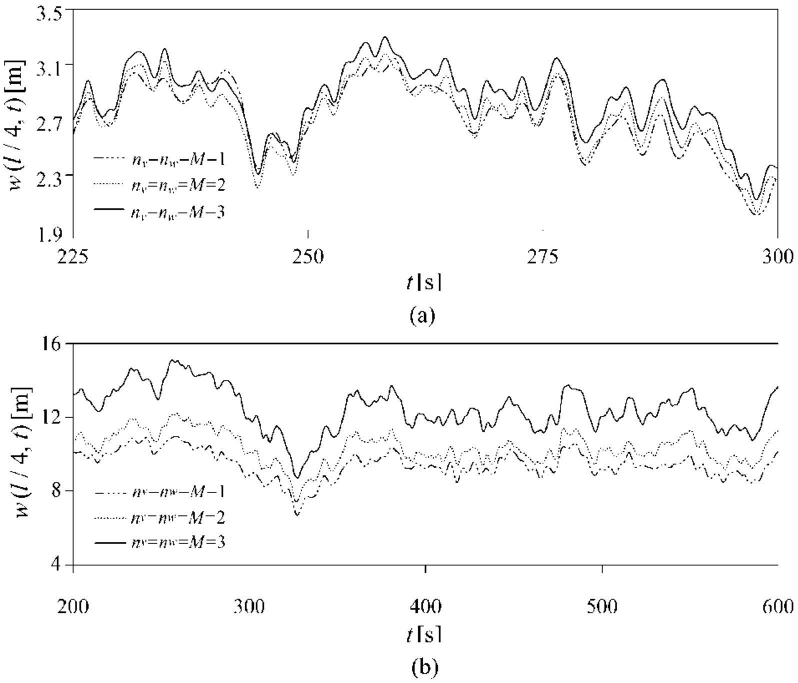


Fig. 7 Samples of out-of-plane vibrations at the quarter-span point obtained retaining one to three cable ($n_v$=$n_w$) and wind ($M$) modes: (a) cable N$^{o}$1 and (b) cable N$^{o}$2

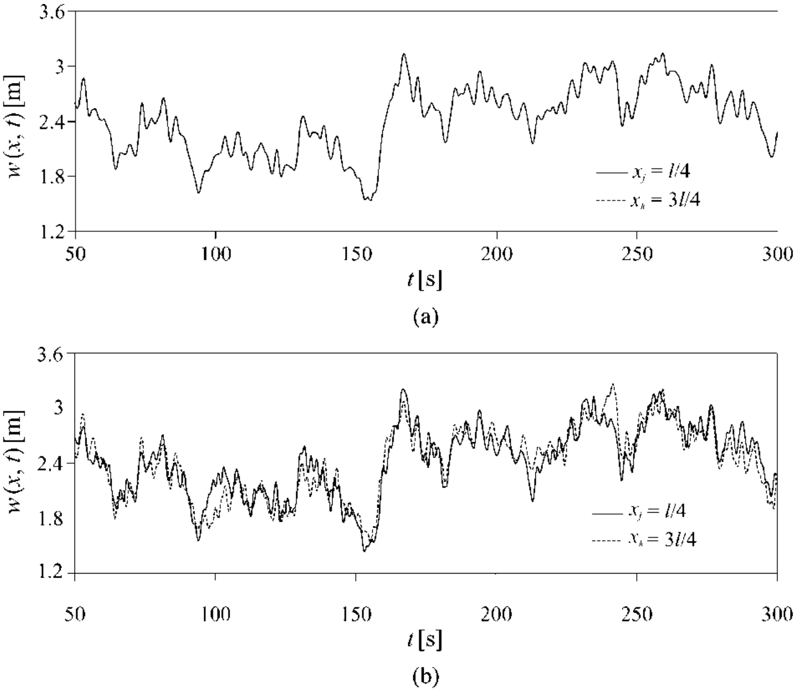


Fig. 8 Samples of out-of-plane vibrations of cable N°1 at $x_j=l/4$ and $x_k=3l/4$: (a) $n_v=n_w=M=1$ and (b) $n_v=n_w=M=2$

$n_v=n_w=M=2$ (Fig. 8b). It can be seen that, if a two-degree-of-freedom discretized model is employed, identical responses at the two point locations are predicted, since as stated previously, for $M=1$ Eq. (24) actually represents a fully coherent random field. Conversely, just the second wind mode and the second swinging cable mode (both antisymmetric) are enough to reveal the loss of coherence between the random processes $w(x_j, t)$ and $w(x_k, t)$. Fig. 9 displays the projection of the steady-state out-of-plane mean configuration plus/minus one standard deviation, $\mu_w \pm \sigma_w$, on the $Oxz$ plane for cables N°1 and N°2. The comparison between the results provided by discretized models of different orders shows once more the fundamental role played by cable and wind modes of higher order than one.

The previous results point out that the effects of spatial correlation of wind velocity fluctuation over long-span suspended cables are quite important. For comparison purposes, the mean value and standard deviation of in-plane ($\mu_v$, $\sigma_v$) and out-of-plane ($\mu_w$, $\sigma_w$) vibrations of the two cables here examined have been computed also under the assumption of uniform wind turbulence. To this aim, a conventional wave superposition-based technique has been employed to simulate the 1V-1D wind velocity process. In order to quantify the effect of spatial correlation, the following percentage error is introduced:

$$\varepsilon_q^{(s)}(\%) = \left| \frac{q_s^{(\mathrm{C})} - q_s^{(\mathrm{U})}}{q_s^{(\mathrm{C})}} \right| \times 100; \qquad q = \mu, \sigma \tag{39}$$

where the subscripts $s=v, w$ denotes in-plane and out-of-plane vibrations; the superscripts in parentheses, C and U, indicate that the response statistic $q$ is evaluated assuming spatially correlated and uniform wind velocity fluctuation, respectively. Tables 2 and 3 list the percentage errors $\varepsilon_q^{(s)}$

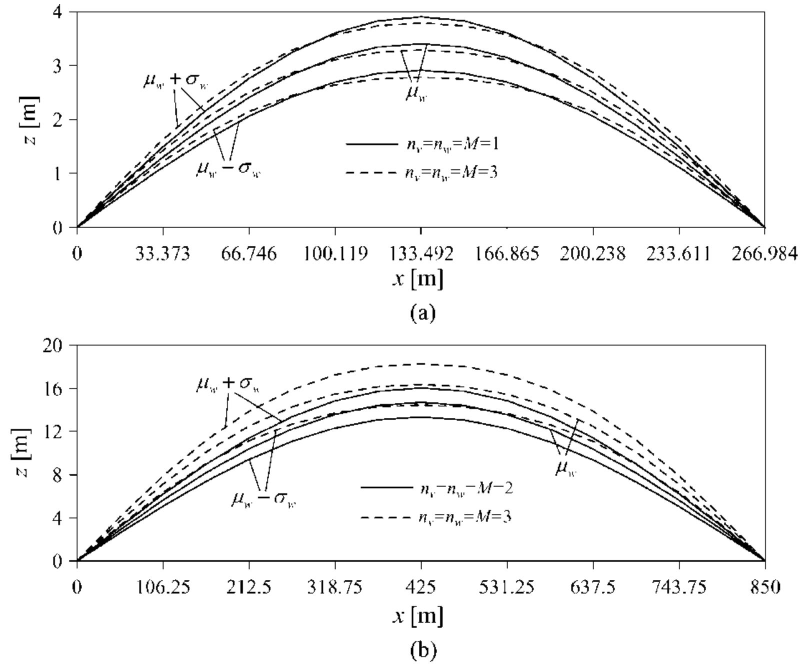


Fig. 9 Steady-state out-of-plane mean configuration plus/minus one standard deviation computed by MCS for two different orders of the Galerkin-type discretized model: (a) cable N^o^ 1 and (b) cable N^o^2

obtained employing Galerkin-type discretized models of different orders for cables N°1 and N°2, respectively. Equally spaced points $x_i=i\Delta x$, $i=1,2,...,7$, with $\Delta x=33.373$ m for the first cable and $\Delta x=106.25$ m for the second one, are considered. According to the concepts outlined above, Table 2 shows that a two-degree-of-freedom discretized model yields constant percentage errors over cable span. It can be seen that both the mean value and standard deviation of in-plane and out-of-plane vibrations are, in general, overestimated when uniform wind turbulence is assumed. An analogous conclusion may be drawn from Fig. 10, which displays the comparison between the projections of

Table 2 Effect of spatial correlation of wind velocity fluctuation upon mean and standard deviation of in-plane and out-of-plane cable displacements at different point locations $x_i$: percentage errors defined by Eq. (39), (Cable N$^0$1)

| $x_i=i\Delta x$ | $n_v=n_w=M=1$ | | | | $n_v=n_w=M=3$ | | | |
|---|---|---|---|---|---|---|---|---|
| | $\varepsilon_\mu^{(v)}$ (%) | $\varepsilon_\mu^{(w)}$ (%) | $\varepsilon_\sigma^{(v)}$ (%) | $\varepsilon_\sigma^{(w)}$ (%) | $\varepsilon_\mu^{(v)}$ (%) | $\varepsilon_\mu^{(w)}$ (%) | $\varepsilon_\sigma^{(v)}$ (%) | $\varepsilon_\sigma^{(w)}$ (%) |
| $x_1$ | 3.7877 | 7.7122 | 139.3087 | 72.7837 | 3.3006 | 0.8985 | 123.6801 | 73.8052 |
| $x_2$ | 3.7877 | 7.7122 | 139.3087 | 72.7837 | 3.4568 | 0.8172 | 131.8017 | 71.8754 |
| $x_3$ | 3.7877 | 7.7122 | 139.3087 | 72.7837 | 3.6221 | 0.7201 | 140.5465 | 69.0385 |
| $x_4$ | 3.7877 | 7.7122 | 139.3087 | 72.7837 | 3.6983 | 0.6598 | 144.5902 | 67.3311 |
| $x_5$ | 3.7877 | 7.7122 | 139.3087 | 72.7837 | 3.6221 | 0.6696 | 140.5465 | 68.0517 |
| $x_6$ | 3.7877 | 7.7122 | 139.3087 | 72.7837 | 3.4568 | 0.7287 | 131.8017 | 70.0074 |
| $x_7$ | 3.7877 | 7.7122 | 139.3087 | 72.7837 | 3.3006 | 0.7886 | 123.6801 | 71.3559 |

Table 3 Effect of spatial correlation of wind velocity fluctuation upon mean and standard deviation of in-plane and out-of-plane cable displacements at different point locations $x_i$: percentage errors defined by Eq. (39), (Cable N$^0$2)

| $x_i = i\Delta x$ | $n_v = n_w = M = 2$ | | | | $n_v = n_w = M = 3$ | | | |
|---|---|---|---|---|---|---|---|---|
| | $\varepsilon_\mu^{(v)}$ (%) | $\varepsilon_\mu^{(w)}$ (%) | $\varepsilon_\sigma^{(v)}$ (%) | $\varepsilon_\sigma^{(w)}$ (%) | $\varepsilon_\mu^{(v)}$ (%) | $\varepsilon_\mu^{(w)}$ (%) | $\varepsilon_\sigma^{(v)}$ (%) | $\varepsilon_\sigma^{(w)}$ (%) |
| $x_1$ | 0.8371 | 1.0358 | 92.9411 | 62.4320 | 1.0426 | 0.9353 | 69.6493 | 70.7444 |
| $x_2$ | 0.8371 | 1.0018 | 92.9411 | 68.1167 | 1.1197 | 0.7804 | 71.7121 | 67.4199 |
| $x_3$ | 0.8371 | 0.9509 | 92.9411 | 73.9280 | 1.1830 | 0.5919 | 75.0675 | 62.3636 |
| $x_4$ | 0.8371 | 0.8908 | 92.9411 | 75.2942 | 1.2176 | 0.4682 | 77.4852 | 59.0249 |
| $x_5$ | 0.8371 | 0.8306 | 92.9411 | 70.3921 | 1.1830 | 0.4735 | 75.0675 | 59.7222 |
| $x_6$ | 0.8371 | 0.7795 | 92.9411 | 62.3431 | 1.1197 | 0.5734 | 71.7121 | 62.6728 |
| $x_7$ | 0.8371 | 0.7453 | 92.9411 | 55.7033 | 1.0426 | 0.6785 | 69.6493 | 64.8673 |

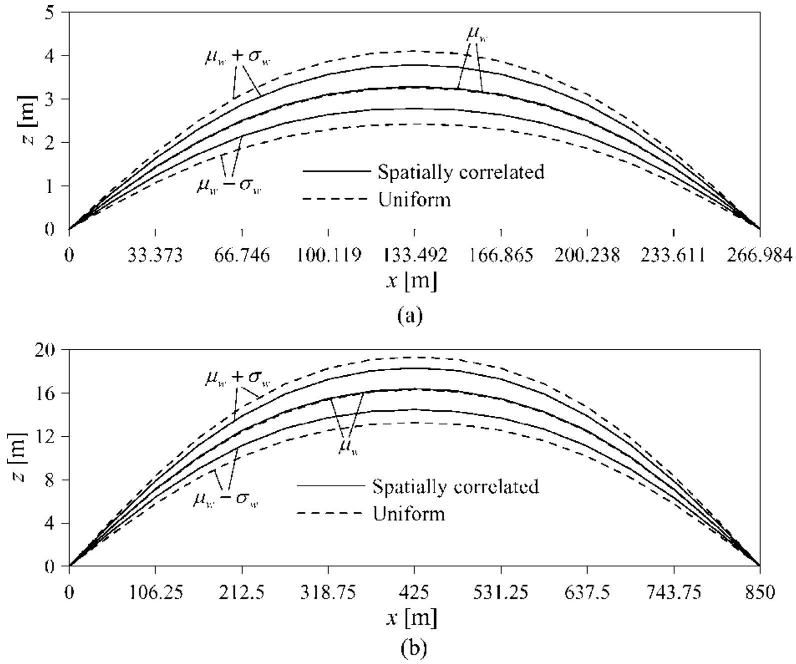


Fig. 10 Effect of spatial correlation of wind velocity fluctuation upon steady-state out-of-plane mean configuration plus/minus one standard deviation ($n_v = n_w = M = 3$): (a) cable N$^o$1 and (b) cable N$^o$2

the steady-state out-of-plane mean configuration plus/minus one standard deviation on the *Oxz* plane, obtained through a six-degree-of-freedom discretized model both including and neglecting spatial correlation of wind turbulence. The previous results show that the widely used model of wind velocity fluctuation as a stationary zero-mean Gaussian random process, uniform over the spatial domain, turns out to be conservative when extended wind-exposed structures, such as long-span suspended cables, are dealt with.

## 5. Conclusions

A Monte Carlo-based approach for analyzing buffeting response of long-span suspended cables has been presented. Aiming at second-order analysis of the response, this procedure fully accounts for geometrical nonlinearities inherent in cable behavior while it neglects nonlinear aerodynamic terms in view of their weak influence on first and second-order statistical moments. By referring the analysis to flat-sag cables, wind velocity fluctuation is treated as a one-variate bi-dimensional zero-mean Gaussian random field, stationary in time and isotropic in space. The time-domain analysis of cable response is carried out through the joint application of the Proper Orthogonal Decomposition of wind turbulence field and Galerkin's discretization of the equations of motion, according to Double Modal Transformation technique. Following a recently proposed approach, the Proper Orthogonal Decomposition of wind velocity fluctuation is performed on the basis of the frequency-dependent eigenfunctions of the CPSD function. So operating, a very efficient technique for digital simulation of the generalized aerodynamic forces is developed. The main drawback of this approach is that it requires the evaluation of the frequency-dependent eigenproperties of the CPSD function, which may be time consuming. However, the similarity detected between the blowing mode shapes and the along-wind linearized eigenfunctions of the cable provides remarkable computational advantages, mainly due to the orthogonality properties shared by wind and cable mode shapes. In particular, by virtue of these properties time-histories of spatially correlated wind loads can be generated via numerical simulation of few one-variate one-dimensional random processes, as many as are the out-of-plane vibration modes of the cable included in the Galerkin-type discretized model. Hence, the cross-correlation of wind velocity fluctuations at different point locations is modeled in a more efficient way than conventional spectral approaches, which rely on the spatial discretization of wind turbulence field itself and the subsequent factorization of the CPSD matrix at each frequency step. Some numerical results have been presented and discussed in the paper, in order to assess the accuracy and efficiency of the proposed simulation procedure. The appropriate selection of the order of the discretized model and the effects of spatial correlation of wind velocity fluctuation on buffeting response have also been investigated through numerical applications.

## Appendix A-Linearized eigenfunctions and natural frequencies of a suspended cable

The symmetric in-plane eigenfunctions and the corresponding natural circular frequencies of a suspended cable are given by Irvine (1981):

$$\varphi_i(x) = A_i\left[1 - \tan\left(\frac{\vartheta_i}{2}\right)\sin(\vartheta_i x) - \cos(\vartheta_i x)\right] \tag{A.1}$$

$$\omega_{vi} = \frac{\vartheta_i}{l}\sqrt{\frac{H}{m}}, \quad (i = 1, 3, 5, \ldots) \tag{A.2}$$

where $A_i$ is a normalization constant and $\vartheta_i$ are the roots of the characteristic equation

$$\tan\left(\frac{\vartheta_i}{2}\right) = \frac{\vartheta_i}{2} - \frac{4}{\lambda^2}\left(\frac{\vartheta_i}{2}\right)^3 \tag{A.3}$$

$\lambda^2=64(EA/H)(d/l)^2$ being the Irvine parameter.

The antisymmetric in-plane eigenfunctions and the associated natural circular frequencies are defined as follows:

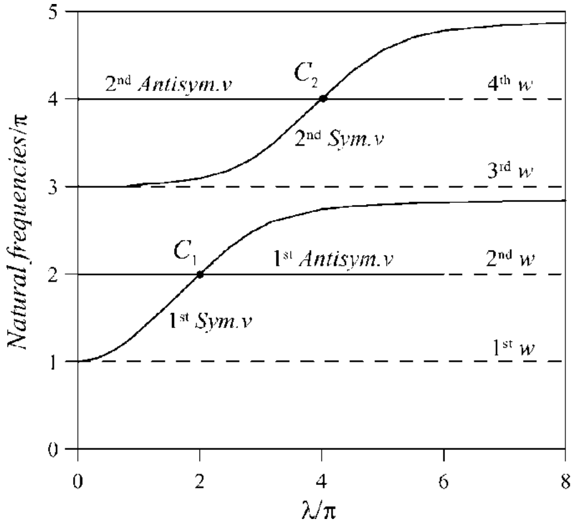


Fig. 11 Dimensionless natural frequencies of in-plane and out-of-plane vibration modes of a suspended cable versus the elasto-geometric parameter $\lambda/\pi$

$$\varphi_i(x) = \sin\left(\frac{i\pi x}{l}\right) \tag{A.4}$$

$$\omega_{vi} = \frac{i\pi}{l}\sqrt{\frac{H}{m}}, \quad (i = 2, 4, 6, ...) \tag{A.5}$$

The out-of-plane eigenfunctions and the corresponding natural circular frequencies are given by:

$$\psi_k(x) = \sin\left(\frac{k\pi x}{l}\right) \tag{A.6}$$

$$\omega_{wk} = \frac{k\pi}{l}\sqrt{\frac{H}{m}}, \quad (k = 1, 2, 3, ...) \tag{A.7}$$

Fig. 11 shows the dependence of the dimensionless natural frequencies $\omega_{vi}(l/\pi)\sqrt{m/H} = \vartheta_i/\pi$ and $\omega_{wk}(l/\pi)\sqrt{m/H} = k$ of in-plane and out-of-plane modes, respectively, on the cable parameter $\lambda/\pi$. For conciseness, *Sym.v* and *Antisym.v* denote the symmetric and antisymmetric in-plane modes, respectively, while the out-of-plane modes are simply indicated by the letter *w*. Notice that only the natural frequencies of the symmetric in-plane modes vary with the elasto-geometric parameter $\lambda/\pi$, as they are the roots of the trascendental equation (A.3). Moreover, internal resonance conditions occur at the crossover points, $C_j$, which are located at $\lambda/\pi=2j$, $(j=1,2,...)$. Physically, the modal crossover phenomenon is explained by the continuous transition from the behavior akin to a taut string to the one of a sagging cable.

## Appendix B-Coefficients of the discretized equations of motion

In order to define the expressions of the coefficients appearing in the discretized equations of motion, the following integrals are first introduced:

$$I_{0,i}^{(v)} = \int_0^l \varphi_i^2(x)\mathrm{d}x; \qquad I_{0,k}^{(w)} = \int_0^l \psi_k^2(x)\mathrm{d}x;$$

$$I_{1,i}^{(v)} = \int_0^l \varphi_i(x)\mathrm{d}x; \qquad I_{1,k}^{(w)} = \int_0^l \psi_k(x)\mathrm{d}x; \tag{B.1}$$

$$I_{2,ij}^{(v)} = \int_0^l \varphi'_i(x)\varphi'_j(x)\mathrm{d}x; \qquad I_{2,k}^{(w)} = \int_0^l \psi'^2_k(x)\mathrm{d}x;$$

where $\varphi_i(x)$ and $\psi_k(x)$ are the in-plane and out-of-plane linearized eigenfunctions of a suspended cable (see Appendix A).

The coefficients $b_j^{(1)}$, $b_{ij}^{(2)}$ and $b_k^{(3)}$ introduced in Eq. (14) are given by:

$$b_j^{(1)} = \frac{8d}{l^3}I_{1,j}^{(v)}; \quad b_{ij}^{(2)} = \frac{I_{2,ij}^{(v)}}{2l}; \quad b_k^{(3)} = \frac{I_{2,k}^{(w)}}{2l} \tag{B.2}$$

while the coefficients $a_{ij}^{(1)}$, $a_i^{(2)}$, $a_{ij}^{(3)}$ and $a_k^{(4)}$ appearing in Eqs. (15) and (16) are defined as:

$$a_{ij}^{(1)} = \frac{H}{m}\frac{I_{2,ij}^{(v)}}{I_{0,i}^{(v)}}; \quad a_i^{(2)} = \frac{8dEA}{l^2 m}\frac{I_{1,i}^{(v)}}{I_{0,i}^{(v)}}; \quad a_{ij}^{(3)} = \frac{EA}{m}\frac{I_{2,ij}^{(v)}}{I_{0,i}^{(v)}}; \quad a_k^{(4)} = \frac{EA}{m}\frac{I_{2,k}^{(w)}}{I_{0,k}^{(w)}} \tag{B.3}$$

Furthermore, under the assumption of mass-proportional damping, $\hat{\mu}_{vi}$ and $\hat{\mu}_{wk}$ (see Eqs. (15) and (16)) are given by:

$$\hat{\mu}_{vi} = 2\zeta_{vi}\omega_{vi} + \frac{\rho C_D b\overline{W}(h)}{2m}; \quad \hat{\mu}_{wk} = 2\zeta_{wk}\omega_{wk} + \frac{\rho C_D b\overline{W}(h)}{m} \tag{B.4}$$

$\zeta_{vi}$ and $\zeta_{wk}$ being the modal damping ratios for the $i$-th in-plane mode and $k$-th out-of-plane mode, respectively. At last, the coefficients $F_{zk}^{(1)}$ and $F_{zk}^{(2)}$ (see Eqs. (17) and (18)) are defined as follows:

$$F_{zk}^{(1)} = \frac{I_{1,k}^{(w)}}{mI_{0,k}^{(w)}}; \quad F_{zk}^{(2)} = \frac{1}{mI_{0,k}^{(w)}} \tag{B.5}$$

## References


Carassale, L., Piccardo, G. and Solari, G. (2001), "Double modal transformation and wind engineering applications", *J. Eng. Mech. ASCE*, **127**(5), 432-439.

Carassale, L. and Solari, G. (2002), "Wind modes for structural dynamics: a continuous approach", *Probab. Eng. Mech.*, **17**, 157-166.

Carassale, L. and Piccardo, G. (2003), "Wind-induced nonlinear oscillations of cables by Volterra approach", *Proceedings of Fifth International Symposium on Cable Dynamics*, Santa Margherita Ligure (Italy), 15-18 September, 149-156.

Davenport, A.G. (1968), "The dependence of wind load upon meteorological parameters", *Proceedings of the International Research Seminar on Wind Effects on Buildings and Structures*, University of Toronto Press, Toronto, (Canada) 19-82.

Deodatis, G. and Shinozuka, M. (1988), "Autoregressive model for non-stationary stochastic processes", *J. Eng. Mech. ASCE*, **114**(11), 1995-2012.

Deodatis, G. (1996), "Simulation of ergodic multivariate stochastic processes", *J. Eng. Mech. ASCE*, **122**(8),

778-787.
Desai, Y.M., Popplewell, N. and Shah, A.H. (1995), "Finite element modelling of transmission lines", *Comput. Struct.*, **57**(3), 407-420.
Di Paola, M. (1998), "Digital simulation of wind field velocity", *J. Wind Eng. Ind. Aerodyn.*, **74-76**, 91-109.
Di Paola, M. and Gullo, I. (2001), "Digital generation of multivariate wind field processes", *Probab. Eng. Mech.*, **16**, 1-10.
Di Paola, M., Muscolino, G. and Sofi, A. (2002), "Nonlinear random vibrations of a suspended cable under wind loading", *Fourth International Conference on Computational Stochastic Mechanics*, Kerkyra (Corfu), Greece 9-12 June, 159-168.
Gattulli, V., Martinelli, L., Perotti, F. and Vestroni, F. (2001), "Nonlinear interactions in cables investigated using analytical and finite element models", *Proceedings of Fourth International Symposium on Cable Dynamics*, Montréal (Canada), 28-30 May, 339-346.
Grigoriu, M. (1993), "Simulation of non-stationary Gaussian processes by random trigonometric polynomials", *J. Eng. Mech. ASCE*, **119**(2), 328-343.
Irvine, H.M. (1981), *Cable Structures*, The MIT Press, Cambridge.
Kaimal, J.C., *et al.* (1972), "Spectral characteristics of surface-layer turbulence", *J. Royal Meteorological Soc.*, London, England, **98**, 563-589.
Li, Y. and Kareem, A. (1990), "ARMA system in wind engineering", *Probab. Eng. Mech.*, **5**(2), 50-59.
Li, Y. and Kareem, A. (1993), "Simulation of multivariate random processes: a hybrid DFT and digital filtering approach", *J. Eng. Mech. ASCE*, **119**(5), 1078-1098.
Li, Y. and Kareem, A. (1995), "Stochastic decomposition and its application to probabilistic dynamics", *J. Eng. Mech. ASCE*, **121**(1), 162-174.
Loeve, M. (1955), *Probability theory*, Van Nostrand, New York.
Luongo, A., Paolone, A. and Piccardo, G. (1998), "Postcritical behavior of cables undergoing two simultaneous galloping modes", *Meccanica*, **33**, 229-242.
Luongo, A., Rega, G. and Vestroni, F. (1984), "Planar non-linear free vibrations of an elastic cable", *Int. J. Non-linear Mech.*, **9**(1), 39-52.
Martinelli, L., Gattulli, V. and Vestroni, F. (2002), "Nonlinear behaviour of a suspended cable under stationary and non-stationary loading", *Proceedings of Fifth International Conference on Structural Dynamics*, Munich (Germany), 2-5 September, 893-898.
Naganuma, T., Deodatis, G. and Shinozuka, M. (1987), "ARMA model for two dimensional processes", *J. Eng. Mech. ASCE*, **113**(2), 234-251.
Papoulis, A. (1965), *Probability, Random Variables and Stochastic Processes*, MacGraw-Hill, New York.
Pasca, M., Vestroni, F. and Gattulli, V. (1998), "Active longitudinal control of wind-induced oscillations of a suspended cable", *Meccanica*, **33**, 255-266.
Piccardo, G. (1993), "A methodology for the study of coupled aeroelastic phenomena", *J. Wind Eng. Ind. Aerodyn.*, **48**(2-3), 241-252.
Priestley, M.B. (1999), *Spectral analysis and time series*, Academic Press, London.
Shinozuka, M. (1971), "Simulation of multivariate and multidimensional random processes", *J. Acoust. Soc. Am.*, **49**(1), 357-367.
Shinozuka, M. and Jan, C. M. (1972), "Digital simulation of random processes and its applications", *J. Sound Vib.*, **25**(1), 111-128.
Shinozuka, M. and Deodatis, G. (1996), "Simulation of multi-dimensional Gaussian stochastic fields by spectral representation", *Appl. Mech. Rev. ASME*, **49**(1), 29-53.
Simiu, E. and Scanlan, R.H. (1996), *Wind Effects on Structures. Fundamentals and Applications to Design*, John Wiley & Sons, Inc New York.
Spanos, P.D. and Mignolet, M.P. (1986), "Z-transform modeling of P-M wave spectrum", *J. Eng. Mech. ASCE*, **192**(8), 745-759.
Spanos, P.D. and Ghanem, R. (1989), "Stochastic finite element expansion for random media", *J. Eng. Mech.*, **115**(5), 1035-1053.
Van Trees, H.I. (1968), *Detection, Estimation and Modulation Theory*, Part 1, vol. 1., Wiley, New York.

*GS*